Glassy Dynamics, Spinodal Fluctuations, and the Kinetic Limit of Nucleation in Suspensions of Colloidal Hard Rods

Ran Ni,[1] Simone Belli,[2] René van Roij,[2] and Marjolein Dijkstra[1]

[1]*Soft Condensed Matter, Utrecht University, Princetonplein 5, 3584 CC Utrecht, The Netherlands*

[2]*Institute for Theoretical Physics, Utrecht University, Leuvenlaan 4, 3584 CE Utrecht, The Netherlands*

(Received 23 March 2010; published 16 August 2010)

Using simulations we identify three dynamic regimes in supersaturated isotropic fluid states of short hard rods: (i) for moderate supersaturations, we observe nucleation of multilayered crystalline clusters; (ii) at higher supersaturation, we find nucleation of small crystallites which arrange into long-lived locally favored structures that get kinetically arrested; and (iii) at even higher supersaturation, the dynamic arrest is due to the conventional cage-trapping glass transition. For longer rods we find that the formation of the (stable) smectic phase out of a supersaturated isotropic state is strongly suppressed by an isotropic-nematic spinodal instability that causes huge spinodal-like orientation fluctuations with nematic clusters diverging in size. Our results show that glassy dynamics and spinodal instabilities set kinetic limits to nucleation in highly supersaturated hard-rod fluids.

DOI: 10.1103/PhysRevLett.105.088302 PACS numbers: 82.70.Dd, 68.55.A−, 82.60.Nh

Nucleation is the process whereby a thermodynamically metastable state evolves into a stable one, via the spontaneous formation of a droplet of the stable phase. From classical nucleation theory (CNT), the Gibbs free energy associated with the formation of a spherical cluster of the stable phase with radius R in the metastable phase is given by $\Delta G = -4\pi R^3 \rho |\Delta\mu|/3 + 4\pi R^2 \gamma$, with γ the surface tension between the coexisting phases, ρ the density of the cluster, and $|\Delta\mu| > 0$ the chemical potential difference between the metastable and stable phase. CNT predicts a nucleation barrier $\Delta G_{\rm crit} = (16\pi/3)\gamma^3/(\rho|\Delta\mu|)^2$ and a critical nucleus radius $R_{\rm crit} = 2\gamma/\rho|\Delta\mu|$. CNT predicts an infinite barrier at bulk coexistence ($\Delta\mu = 0$), which decreases with increasing supersaturation. However, CNT incorrectly predicts a *finite* barrier at the spinodal, whereas a nonclassical approach yields a vanishing barrier at the spinodal, with a diffuse critical nucleus that becomes of infinite size [1]. Both approaches explain why liquids must be supercooled substantially before nucleation occurs, and one might expect that nucleation should always occur for sufficiently high supersaturation. For deep quenches of soft spheres close to a spinodal, but not beyond it, simulation studies show either nucleating anisotropic and diffuse clusters or precritical clusters that grow further or that coalesce in ramified structures [2]. These results contrast the mean-field predictions that the critical size should diverge at the spinodal [1]. Wedekind *et al.* showed that a Lennard-Jones system can become unstable by a so-called kinetic spinodal, where the largest cluster in the system has a vanishing barrier, i.e., $\Delta G_{\rm crit}^{\rm large} = 0$, implying the immediate formation of a critical cluster in the system [3]. Beyond this kinetic limit, which is system-size-dependent as $\Delta G_{\rm crit}^{\rm large} = \Delta G_{\rm crit} - k_B T \ln N$, the system is kinetically unstable, and the phase transformation proceeds immediately via growth of the largest cluster. Here N is the number of particles, k_B the Boltzmann constant, and T the temperature. This scenario also explains why it is hard to reach the thermodynamic spinodal and why a divergence of the critical cluster size is never observed in simulations, as the system already becomes kinetically unstable at much lower supersaturations. Interestingly, recent simulations of silica also showed a kinetic limit of the homogeneous nucleation regime that is strongly influenced by glassy dynamics, without any spinodal effects [4]. Clearly, the nucleation kinetics at high supersaturation is still poorly understood.

In this Letter, we investigate the nucleation pathways of the isotropic-crystal (IX) transition of rodlike particles as a function of supersaturation and those of the isotropic-smectic (ISm) transition. The nucleation pathways of structures with both orientational and positional order are still unknown, as nucleating smectic or crystalline clusters have never been observed in experiments or simulations [5,6]. We show for the first time that IX nucleation proceeds via multilayer nuclei, while previous studies found that nucleation is hampered by self-poisoning [5]. Additionally, we identify two mechanisms of dynamic arrest that set a kinetic limit to the IX nucleation regime, one based on dynamic arrest of small crystalline nuclei that form locally favored structures and one based on a conventional cage-trapping glass transition. Moreover, for longer rods we show that the isotropic-nematic (IN) spinodal associated with a metastable IN transition severely hinders and even prevents ISm nucleation.

We consider a suspension of N hard spherocylinders with a diameter σ and a cylindrical segment of length $L = 2\sigma$ in a volume V or at pressure P. The bulk phase diagram of these rods with a length-to-diameter ratio $L^* = L/\sigma = 2$ is well known [7]; it features an IX transition at pressure $P^* = \beta P \sigma^3 = 5.64$, with $\beta = 1/k_B T$.

We first use *NPT* Monte Carlo (MC) simulations to compress an isotropic fluid of 10 000 rods at the moderate pressure $P^* = 7.6$ corresponding to a chemical potential

difference $\beta|\Delta\mu| = 1.11$ between the (metastable) fluid and the crystal phase. We then take random MC configurations as initial configurations for molecular dynamics (MD) simulations in the *NVT* ensemble to study spontaneous crystal nucleation, employing the cluster criterion as described in Refs. [8,9]. We find spontaneous nucleation of a multilayered crystalline cluster in the isotropic fluid. Figure 1(a) shows the time evolution from a typical MD trajectory. In the initial stage of the MD simulation, the system remains in the metastable isotropic fluid for a long time. After time $t = 1000\tau$, with $\tau = \sigma\sqrt{m/k_BT}$ and m the mass of the particle, a nucleus consisting of multiple crystalline layers starts to grow gradually until the whole system has been transformed into the bulk crystal phase. We note that the cluster prefers to grow laterally as was also found for attractive rods [6]. We observed similar spontaneous nucleation at $P^* = 7.4$. The long waiting time t_w before a postcritical cluster appears by a spontaneous fluctuation is typical for nucleation and growth. We calculate the nucleation rate $R = 1/\langle t_w\rangle V$ and find from MD simulations that $R\sigma^3\tau = 5 \times 10^{-9\pm2}$ and $1.7 \times 10^{-8\pm1}$, for $P^* = 7.4$ and 7.6, respectively.

As our MD simulations provide evidence that the IX transformation can occur via nucleation of multilayer crystalline clusters, we determine the nucleation barrier by using umbrella sampling (US) in MC simulations [8]. We perform MC simulations of 2000 particles at $P^* = 7.0$, 7.2, and 7.4 corresponding to $\beta|\Delta\mu| = 0.78$, 0.89, and 1.0, respectively. Figure 1(b) shows $\Delta G(n)$, which for $P^* = 7.2$ and 7.4 displays a maximum of $\beta\Delta G_{\rm crit} \approx 27 \pm 1.5$ and 20 ± 1.5 at critical cluster sizes $n_{\rm crit} \approx 140$ and 80, respectively. A typical configuration of the critical cluster, consisting of three crystalline layers at $P^* = 7.4$, is shown in the inset in Fig. 1(b); its structure agrees with those observed in our MD simulations of spontaneous nucleation of multilayer crystallites. For $P^* = 7.0$ the free-energy barrier is too high to be calculated in our simulations as the cluster starts to percolate the simulation box before the top is reached. For lower pressures, i.e., $P^* = 6.0$ (not shown), this problem is even more severe. For clusters up to $n \simeq 100$, the barrier can be calculated with the US scheme, revealing multilayered structures very similar to the one shown for $P^* = 7.4$. Our MC simulation results for $P^* = 7.2$ and 7.4 can also be used to calculate the nucleation rate from $R = \kappa\exp(-\beta\Delta G_{\rm crit})$ with kinetic prefactor $\kappa = |\beta\Delta G''_{\rm crit}/(2\pi)|^{1/2}\rho_{\rm I} f_{n_{\rm crit}}$, with $\rho_{\rm I}$ the number density of the isotropic fluid and $f_{n_{\rm crit}}$ the attachment rate of particles to the critical cluster (which we compute by using MD simulations starting with independent configurations at the top of the nucleation barrier [10]). For $P^* = 7.2$ and 7.4 we find $R\sigma^3\tau = 1 \times 10^{-13\pm1}$ and $2 \times 10^{-10\pm1}$, respectively, in agreement within error bars with the MD simulations.

Our observation of bulk crystal nucleation of short rods is in marked contrast with an earlier study, which showed that the free energy never crosses a nucleation barrier [5]. These simulations showed the formation of a single crystalline layer, while subsequent crystal growth is hampered. The authors attributed the stunted growth of this monolayer to self-poisoning by rods that lie flat on the cluster surface. If we use the same cluster criterion as in Ref. [5] for the biasing potential, we indeed find crystalline monolayers at $P^* = 7.4$, which cannot grow further as $\Delta G(n)$ increases monotonically with n. These results for the nucleation barrier agree with theoretical predictions that for sufficiently low supersaturations $\Delta G(n)$ for a single layer is always positive, while multilayer crystalline clusters can grow spontaneously when the nucleus exceeds the critical size [11]. However, our detailed check [9] of the order parameter in Ref. [5] actually reveals a strong (unwanted) bias to form single-layered clusters in US simulations.

We also study the IX transformation at higher supersaturation. To this end, we compress 1000 rods ($L^* = 2$) in *NPT*-MC simulations at $P^* = 8$ ($\beta|\Delta\mu| = 1.33$). Using $\beta\gamma\sigma^2 \simeq 0.44$, which follows from fitting the two barriers of Fig. 1(b) to CNT, we estimate barriers as low as $\beta\Delta G_{\rm crit} \sim 12$ and $\beta\Delta G^{\rm large}_{\rm crit} \sim 5$ for $P^* = 8$. Indeed, many small crystallites nucleate immediately after the compression quench, indicative of the proximity of a kinetic spinodal. These crystallites are oriented in different directions and have a large tendency to orient perpendicular to each other. The subsequent equilibration is extremely

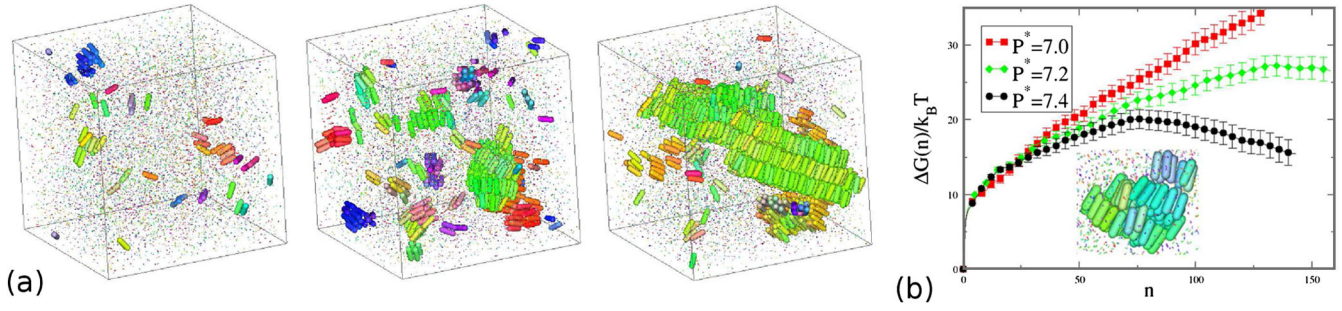

FIG. 1 (color online). (a) Configurations for spontaneous crystal nucleation from a typical molecular dynamics trajectory at $P^* = 7.6$ and $t/\tau = 0$, 1000, and 3000 (from left to right). Isotropiclike particles are drawn 10 times smaller than their actual size. A movie can be found in Ref. [9]. (b) Gibbs free energy $\Delta G(n)$ as a function of the number of rods n in the crystalline cluster at pressure $P^* = 7.0$, 7.2, and 7.4. Inset: A typical configuration of a critical cluster ($n = 81$) at $P^* = 7.4$.

slow, since the growth of a single crystal evolves via collective rearrangements of smaller clusters that subsequently coalesce. In fact, after 3×10^7 MC cycles, our system is dynamically arrested. Interestingly, Frank proposed more than 50 years ago that dynamic arrest may be attributed to the formation of *locally favored structures* (LFS) in which the system gets kinetically trapped in local potential-energy minima [12], while direct observation of such a mechanism for dynamic arrest was only recently reported in the gel phase of a colloid-polymer mixture [13]. In our simulations, we clearly observe the formation of long-lived LFS consisting of perpendicularly oriented crystallites. Only via cooperative rearrangements (rotation of the whole cluster) can the system escape from the kinetic traps, but these events are rare in MC simulations. So, despite the large supersaturation and the low barrier as predicted by CNT, the actual formation of a single crystal is impeded dramatically by slow dynamics. Our observations agree with experiments on soft-repulsive selenium rods, where transient structures of 5–10 aligned particles tend to form LFS with perpendicularly oriented clusters, which gradually merge into larger clusters [14].

To investigate whether the system can be quenched *beyond* a thermodynamic spinodal (such that the transformation proceeds via spinodal decomposition), we perform simulations at $P^* = 10$. We find again the immediate nucleation of many small crystallites, as expected beyond the kinetic spinodal. As the phase transformation sets in right away, we cannot determine whether the nucleation barrier is finite or zero; it is therefore unclear whether or not we have crossed a thermodynamic spinodal (if there is one for freezing). However, we did not find any characteristics of early-stage spinodal decomposition. The small crystallites tend to orient perpendicularly, and the system displays clear orientational ordering along three perpendicular directions (cubatic order), as shown by the orientation distribution on the surface of a unit sphere in the inset

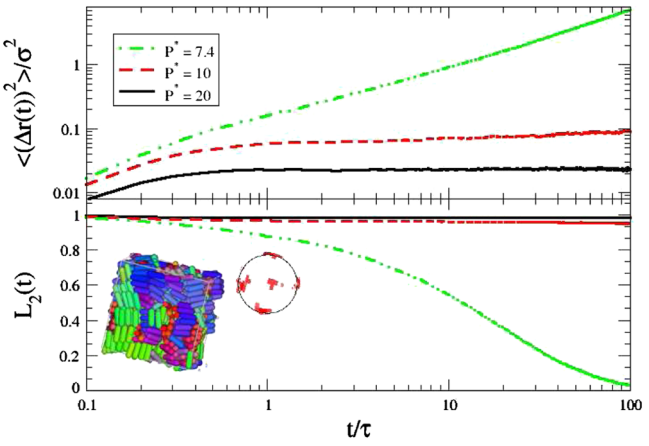

FIG. 2 (color online). Mean-square displacement $\langle[\Delta\mathbf{r}(t)]^2\rangle$ and second-order orientational correlator $L_2(t)$ for hard rods with $L^* = 2$ and pressures as labeled. The inset shows a typical configuration of a glassy state with cubatic order at $P^* = 10$.

in Fig. 2. To check for finite size effects, we studied a system of $N = 4000$ rods, which again shows system-spanning cubatic order. Whether or not the cubatic order is long-ranged for even larger systems remains unsettled. The mean-square displacement $\langle[\Delta\mathbf{r}(t)]^2\rangle$ and the second-order orientational correlator $L_2(t) = \langle[3\cos^2\theta(t) - 1]/2\rangle$ are displayed in Fig. 2, which shows the characteristic plateau of structural arrest. For comparison, we also present data for $P^* = 7.4$, which show relatively fast relaxation of the translational and orientational degrees of freedom. At an even larger supersaturation $P^* = 20$, we find that the system is kinetically arrested immediately after the quench. We find hardly any crystalline order, while the orientation distribution remains isotropic (not shown). Clearly, the system crossed the conventional cage-trapping glass transition [15] that prevents the formation of any ordering. The dynamic arrest can be appreciated by the plateau in $\langle[\Delta\mathbf{r}(t)]^2\rangle$ and $L_2(t)$ in Fig. 2. Our results thus show that nucleation at high supersaturation is strongly affected by vitrification, either due to LFS or by the conventional glass transition, yielding glasses with and without small crystallites, respectively.

We also study longer hard rods with $L^* = 3.4$, which show ISm coexistence at $P^* = 2.828$. A previous MC simulation study [16] showed the formation of the smectic phase out of the highly supersaturated I phase at $P^* = 3.1$ via spinodal decomposition. However, nucleation and growth of the smectic phase out of weakly supersaturated I phases at $P^* = 2.85$–3.0 was *not* observed [16]. As strong presmectic ordering and huge nematiclike clusters were observed in the I phase, the hampered nucleation was attributed to slow dynamics. Here we reinvestigate the regime $P^* = 2.828$–3.0 at much longer time scales by MD simulations. We confirm the earlier findings of the structure but do not find any evidence for structural arrest in $\langle[\Delta\mathbf{r}(t)]^2\rangle$ and $L_2(t)$ (not shown). Instead, we find huge and strongly fluctuating nematiclike clusters [9]. The nematic character of the clusters is evident from the structure factor $S(k)$ and orientational structure factor $S_{or}(k)$, shown in Fig. 3, revealing a small-k divergence for $S_{or}(k)$ but not for $S(k)$ [15]. The correlation length ξ of the orientational fluctuations obtained from fitting the orientational correlation function $g_{or}(r) \sim \exp(-r/\xi)/r$ is shown in the inset to satisfy a power law $\xi \sim |P - P_c|^{-\nu}$, with $P_c^* = 3.01$ the alleged IN-spinodal pressure and $\nu = 0.47$, which is close to the expected mean-field exponent $\nu = 1/2$ of the IN spinodal [17]. Apparently, the ISm nucleation is prevented by an intervening IN spinodal. Our observation that the metastable isotropic fluid is more susceptible to nematic than to smectic fluctuations is corroborated by second-virial calculations of the Zwanzig model of blocklike $H \times D \times D$ rods with three orthogonal orientations [9]. The dimensionless Helmholtz free-energy density F/V of the I, N, and Sm phases for $H/D = 4.3$, shown in Fig. 3, reveal equilibrium ISm coexistence and a metastable N branch. The IN spinodal on the metastable isotropic branch occurs at a lower packing fraction η than the ISm spinodal. In

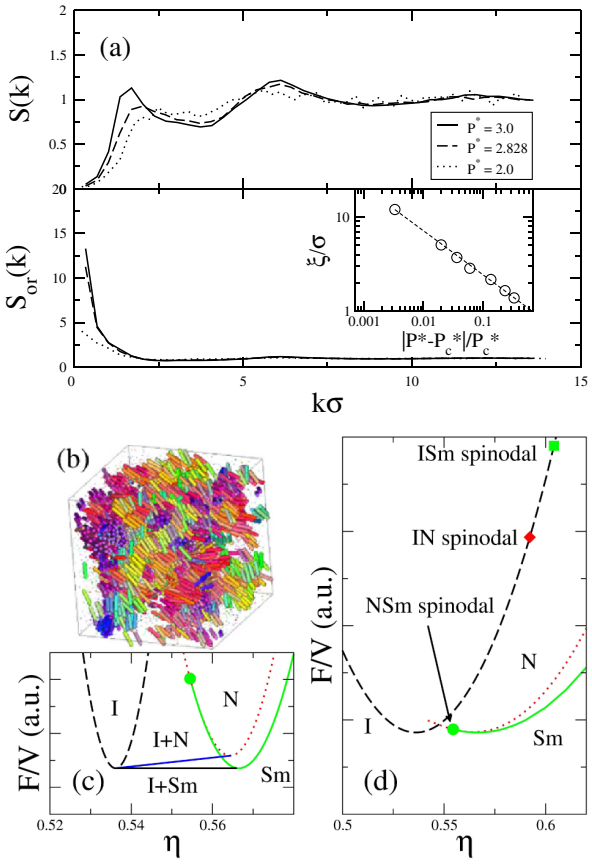

FIG. 3 (color online). (a) Positional (top) and orientational (bottom) structure factor of hard rods with $L/\sigma = 3.4$ at varying P^*. The inset shows the pressure dependence of the orientation correlation length ξ. The dashed line is the power-law fitting $\xi \sim |P - P_c|^{-\nu}$. (b) Typical configuration at $P^* = 3$. A movie is shown in Ref. [9]. Isotropiclike particles are drawn 10 times smaller than their actual size. (c),(d) Conveniently shifted and scaled Helmholtz free-energy density F/V of Zwanzig rods (packing fraction η, aspect ratio $H/D = 4.3$) in the I (dashed), N (dotted), and Sm (green) phases. ISm and metastable IN coexistence are indicated by the solid lines, and the IN and ISm spinodal instabilities are denoted by the symbols on the supersaturated isotropic free-energy branch.

other words, the isotropic fluid is predicted to exhibit spinodal nematic fluctuations upon increasing the supersaturation, consistent with the diverging ξ as observed in our simulations. One might expect that the presence of these nematic clusters facilitates the formation of the smectic phase. However, although we find some layering of the rods, the density within these nematic clusters is too low and the orientational fluctuations change too rapidly to form the smectic layers.

In conclusion, our results show that nucleation of hard rods from a supersaturated isotropic fluid phase to crystal and smectic phases is much more rare than perhaps naively anticipated. Only for very short rods and moderate supersaturations do we find nucleation of multilayered crystals; at higher supersaturations, we identified two mechanism for dynamic arrest. The first one occurs close to the kinetic spinodal, where (locally favored) crystalline clusters appear immediately after the quench, followed by slow dynamics due to geometric constraints of these tightly packed clusters. The second type of dynamic arrest occurs at very high supersaturation and is due to the conventional cage-trapping glass transition. In the supersaturated isotropic state of longer rods ($L^* = 3.4$), the nucleation of the (equilibrium) smectic phase is found to be hampered by nematic fluctuations due to the existence of an IN-spinodal instability. We showed for the first time that for quenches close to a spinodal the clusters diverge in size. Our findings are of fundamental and practical interest. They provide strong evidence for a local structural mechanism for dynamic arrest in a system with orientational and positional degrees of freedom. They also explain why the self-organization of ordered assemblies of nanorods is difficult and why most of the nanorod self-assembly techniques require additional alignment of the rods by applied electric fields, fluid flow, or substrates in order to facilitate the formation of the desired self-assembled structures [18]. Our simulations show that this additional "steering" is required since the spontaneous nucleation of the rods is strongly affected by glassy dynamics and spinodal instabilities.

Financial support of a NWO-VICI grant is acknowledged. This work is part of the research program of FOM, which is financially supported by NWO.

[1] K. Binder, Phys. Rev. A **29**, 341 (1984).
[2] H. Wang, H. Gould, and W. Klein, Phys. Rev. E **76**, 031604 (2007); F. Trudu, D. Donadio, and M. Parrinello, Phys. Rev. Lett. **97**, 105701 (2006); P. Bhimalapuran, S. Chakrabarty, and B. Bagchi, Phys. Rev. Lett. **98**, 206104 (2007).
[3] J. Wedekind *et al.*, J. Chem. Phys. **131**, 114506 (2009).
[4] I. Saika-Voivod, R. K. Bowles, and P. H. Poole, Phys. Rev. Lett. **103**, 225701 (2009).
[5] T. Schilling and D. Frenkel, Phys. Rev. Lett. **92**, 085505 (2004).
[6] A. Patti and M. Dijkstra, Phys. Rev. Lett. **102**, 128301 (2009).
[7] P. Bolhuis *et al.*, J. Chem. Phys. **106**, 666 (1997).
[8] A. Cuetos and M. Dijkstra, Phys. Rev. Lett. **98**, 095701 (2007).
[9] See supplementary material at http://link.aps.org/supplemental/10.1103/PhysRevLett.105.088302 for movies and technical details.
[10] S. Auer *et al.*, Nature (London) **409**, 1020 (2001).
[11] D. Frenkel and T. Schilling, Phys. Rev. E **66**, 041606 (2002).
[12] F. C. Frank, Proc. R. Soc. A **215**, 43 (1952).
[13] C. P. Royall *et al.*, Nature Mater. **7**, 556 (2008).
[14] H. Maeda and Y. Maeda, Phys. Rev. Lett. **90**, 018303 (2003).
[15] M. Letz and A. Latz, Phys. Rev. E **60**, 5865 (1999).
[16] A. Cuetos *et al.*, Faraday Discuss. **144**, 253 (2010).
[17] E. F. Gramsbergen *et al.*, Phys. Rep. **135**, 195 (1986).
[18] D. Baranov *et al.*, Nano Lett. **10**, 743 (2010).

Supplementary information
Glassy dynamics, spinodal fluctuations, and the kinetic limit of hard-rod nucleation

Ran Ni[1], Simone Belli[2], René van Roij[2], and Marjolein Dijkstra[1]

[1]*Soft Condensed Matter, Utrecht University,*

Princetonplein 5, 3584 CC Utrecht, The Netherlands and

[2]*Institute for Theoretical Physics, Utrecht University,*

Leuvenlaan 4, 3504 CE, Utrecht, The Netherlands

(Dated: June 29, 2010)

I. CLUSTER CRITERION USED IN THIS WORK

In order to follow a phase transformation, a cluster criterion is needed that is able to identify the new phase from the supersaturated phase. For spherical particles several cluster criteria have been defined to study nucleation. The cluster criterion that is proposed in Ref. [1] to study gas-liquid nucleation, consists of (i) identifying all particles with a liquid-like environment (i.e. particles that have a local density that is significantly higher than that of the vapour) and (ii) applying the criterion that two liquid-like particles belong to the same cluster when they are sufficiently close to each other. Similarly, for the liquid-solid transformation, the cluster criterion in Ref. [2] is based on (i) identifying all particles with a solid-like environment using the local bond orientational order parameters, and ii) applying the criterion that two solid-like particles belong to the same cluster if they are sufficiently close. Our cluster criterion that we developed to study nucleation of hard spherocylinders with a length-to-diameter ratio of L/σ is within the same spirit [3]: We first identify all particles that have an orientationally ordered environment. Subsequently, orientationally ordered particles that are sufficiently close and aligned to each other belong to the same cluster. To this end, we first define the local environment of particle i by all particles j with a surface-to-surface distance $\rho_{ij} < 1.5\sigma$. The local orientational order of particle i is defined by

$$S(i) = \frac{1}{n_i} \sum_{j=1}^{n_i} \left(\frac{3}{2} |\mathbf{u}_j \cdot \mathbf{u}_i|^2 - \frac{1}{2} \right), \tag{1}$$

where $\mathbf{u}_j$ is the unit orientation vector of particle j and n_i is the number of particles with a surface-to-surface distance $\rho_{ij} < 1.5\sigma$. We have adopted the criterion that particle i is orientationally ordered if $S(i) > 0.4$. After identifying the orientationally ordered particles in the system, we determine the cluster using the criterion that two orientationally ordered particles i and j belong to the same cluster if $\rho_{ij} < 0.5\sigma$ and $|\mathbf{u}_i \cdot \mathbf{u}_j| > 0.7$.

II. CLUSTER CRITERION IN REF [4]

The cluster criterion that was proposed in Ref. [4] is much simpler and assumes that two particles i and j belong to the same cluster if $\rho_{ij} < 0.5\sigma$ and $|\mathbf{u}_i \cdot \mathbf{u}_j| > 0.995$.

In order to check this cluster criterion, we performed umbrella sampling Monte Carlo simulations at a reduced pressure $P^* = \beta P/\sigma^3 = 7.4$ for a system of hard spherocylinders

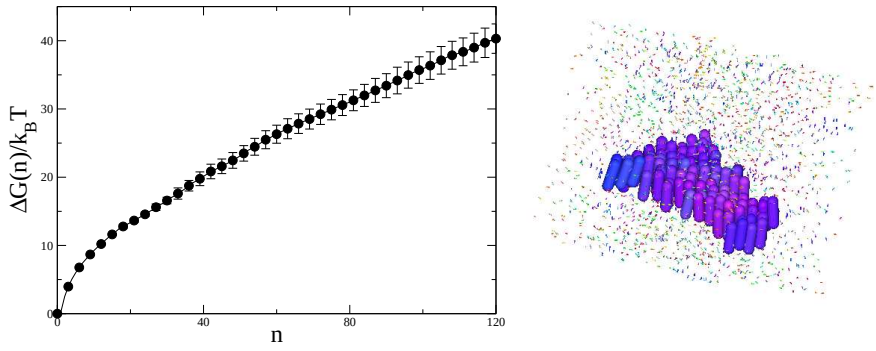

FIG. S1: Gibbs free energy $\beta\Delta G(n)$ as a function of cluster size n (left) and a typical cluster configuration consisting of $n = 95$ particles (right) obtained from umbrella sampling Monte Carlo simulations using the biasing potential proposed in Ref. [4].

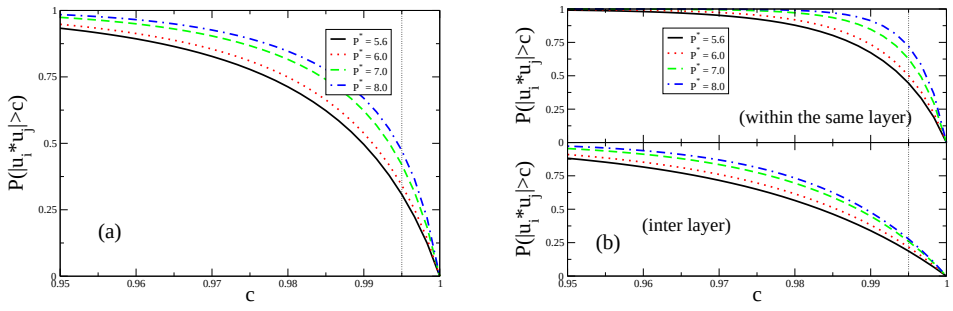

FIG. S2: (a) Probability distribution function $P(|\mathbf{u}_i \cdot \mathbf{u}_j| > c)$ as a function of c for particles i and j with a surface-to-surface distance $\rho_{ij} < 0.5\sigma$ in a bulk crystal phase at pressure $P^* = 5.6, 6.0, 7.0,$ and 8.0. (b) $P(|\mathbf{u}_i \cdot \mathbf{u}_j| > c)$ as a function of c for particles i and j within the same crystalline layer (top) and in different layers (bottom), and a surface-to-surface distance $\rho_{ij} < 0.5\sigma$.

with $L^* = L/\sigma = 2$ using the biasing potential of Ref. [4]. The Gibbs free energy $\beta\Delta G(n)$ as a function of cluster size n is shown in Fig. S1 along with a typical configuration of a cluster of size $n = 95$. We clearly observe that $\beta\Delta G(n)$ increases monotonically with n and never crosses a nucleation barrier in agreement with the findings of Ref. [4]. Additionally, we find that only monolayered crystals are formed, which cannot grow further as $\beta\Delta G(n)$ increases with n.

In order to investigate why the criterion seems to bias towards monolayered clusters, we calculated for an equilibrated bulk crystal at reduced pressures $P^* = 5.6, 6.0, 7.0,$ and 8.0,

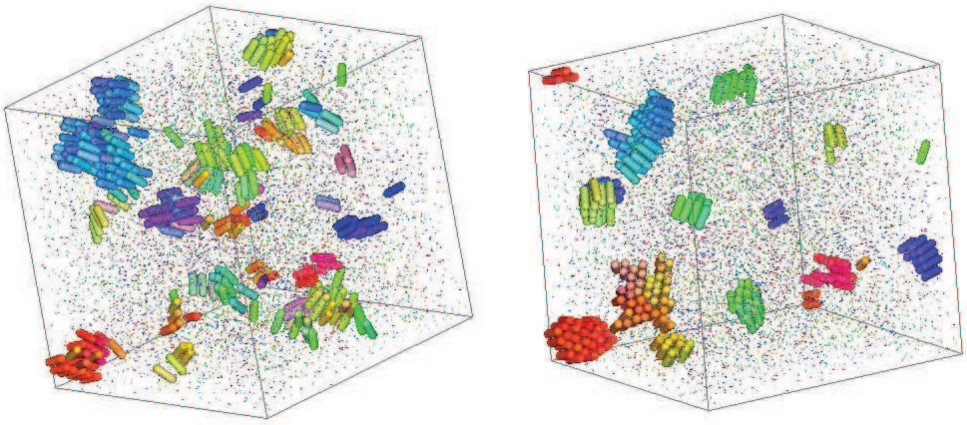

FIG. S3: (left) Precritical clusters identified using the cluster criterion in the present work, which are multicrystalline. (right) The cluster criterion of Ref. [4] is only able to detect monolayer crystallites in the same configuration.

the probability distribution of $P(|\mathbf{u}_i \cdot \mathbf{u}_j| > c)$ as a function of c for all particle pairs that satisfy $\rho_{ij} < 0.5\sigma$. Fig. S2(a) shows that only 30-50 % of these particles in the bulk crystal phase are recognized as crystalline by the criterion $|\mathbf{u}_i \cdot \mathbf{u}_j| > 0.995$ as was used in Ref. [4]. We also determined $P(|\mathbf{u}_i \cdot \mathbf{u}_j| > c)$ for particles with $\rho_{ij} < 0.5\sigma$ within the same crystalline layer and in different layers in Fig. S2(b), respectively. We find that $40 - 70\%$ of the particles are defined to be crystalline within the same layer, while only $15 - 25\%$ between the layers. Hence, the cluster criterion of Ref. [4] reveals a severe (unwanted) bias towards monolayer clusters in umbrella sampling simulations.

In addition, we employed our cluster criterion and that of Ref. [4] to analyze the structure of precritical clusters that already appear occasionally in the supersaturated fluid phase without using any biasing potential. Fig. S3 shows that the cluster criterion of Ref. [4] only detects monolayer crystals, while our cluster criterion already finds multi-layered crystals, although very small, in the same configuration.

In conclusion, a good cluster criterion should be able to identify all the particles in a well-equilibrated system of the new bulk phase, while it detects only a very small number of tiny clusters in the supersaturated parent phase. An additional check would be to investigate whether the cluster criterion can already identify precritical clusters in the supersaturated bulk phase using unbiased Monte Carlo or Molecular Dynamics simulations.

III. ZWANZIG MODEL FREE-ENERGY CALCULATIONS

A. Second-virial functional

In order to support our simulation result that the supersaturated isotropic phase of hard spherocylinders with $L^* = 3.4$ becomes unstable with respect to nematic rather than smectic fluctuations, we also perform free-energy calculations and stability analyses within a density functional theory for a system of hard parallelepipeds with sides $H \times D \times D$ and $H/D = 4.3$. For the sake of simplicity the rotational degrees of freedom of the rods were described according to the so-called Zwanzig model, in which a particle can assume only three mutually orthogonal orientations [5]. Despite its simplicity, this model captures the essential physics of hard-rod fluids, since, for instance, its bulk phase diagram [6] and its wetting and capillarity behavior is very similar to that of freely rotating hard rods [7]. We define the one-particle distribution (o.p.d.) $\rho_\alpha(\mathbf{r})$ (with $\alpha \in \{x, y, z\}$) of rods with center-of-mass position $\mathbf{r}$ whose long axis is aligned along axis α of a fixed Cartesian reference frame. For a bulk system of N particles in a volume V the o.p.d. satisfies the normalization condition

$$\sum_\alpha \int_V d\mathbf{r} \rho_\alpha(\mathbf{r}) = N, \tag{2}$$

where the α-summation is over all three possible orientations. In the formalism of density functional theory the (intrinsic) Helmholtz free energy F of the system is expressed as a functional of the o.p.d. [8]. Within the second-virial approximation one writes $F[\rho]$ as a sum of an ideal-gas and an $\mathcal{O}(\rho^2)$ interaction term,

$$\begin{aligned} \beta F[\rho] \;=\; & \sum_\alpha \int_V d\mathbf{r} \{\rho_\alpha(\mathbf{r})[\log(\rho_\alpha(\mathbf{r})) - 1]\} \\ & - \frac{1}{2} \sum_{\alpha,\alpha'} \int d\mathbf{r} d\mathbf{r}' f_M^{\alpha\alpha'}(\mathbf{r}, \mathbf{r}') \rho_\alpha(\mathbf{r}) \rho_{\alpha'}(\mathbf{r}'), \end{aligned} \tag{3}$$

where $\beta = 1/k_B T$ and $f_M^{\alpha\alpha'}(\mathbf{r}, \mathbf{r}') = \exp[-\beta u_{\alpha\alpha'}(\mathbf{r}, \mathbf{r}')] - 1$ the Mayer function in terms of the pair interaction $u_{\alpha\alpha'}(\mathbf{r}, \mathbf{r}')$ between two rods with orientations α and α' at positions $\mathbf{r}$ and $\mathbf{r}'$. For the hard bodies of interest here, $f_M = -1$ and 0 for overlapping and non-overlapping pairs of rods, respectively.

B. Minimization

At a fixed temperature T and density $n = N/V$, the equilibrium o.p.d. minimizes $F[\rho]$ with the constraint that the normalization condition (2) be satisfied. This gives rise to the self-consistency equation

$$\rho_\alpha(\mathbf{r}) = C \exp[\sum_{\alpha'} \int_V d\mathbf{r}' f_M^{\alpha\alpha'}(\mathbf{r}, \mathbf{r}')\rho_{\alpha'}(\mathbf{r}')], \tag{4}$$

whose solutions are candidates for the equilibrium o.p.d. The constant C is fixed by the normalization condition (2). Here we only consider solutions that satisfy translation-invariance in the $x-y$ plane (which includes the symmetries of isotropic, nematic, and smectic phases), such that we can write $\rho_\alpha(\mathbf{r}) = \rho_\alpha(z)$. Assuming a periodicity λ in the z-direction, we can expand the o.p.d. as a Fourier series

$$\rho_\alpha(z) = \frac{\rho_{\alpha 0}}{2} + \sum_{k=1}^{\infty} \rho_{\alpha k} \cos[\frac{2\pi k}{\lambda} z], \tag{5}$$

the coefficients of which satisfy

$$\rho_{\alpha k} = \frac{2}{\lambda} \int_{-\lambda/2}^{\lambda/2} dz \rho_\alpha(z) \cos[\frac{2\pi k}{\lambda} z]. \tag{6}$$

Inserting the Fourier modes into the minimum condition (4) yields

$$\rho_\alpha(z) = C \exp\{\sum_{\alpha'} [F^{\alpha\alpha'}(0)\frac{\rho_{\alpha' 0}}{2} + \sum_{k=1}^{\infty} F^{\alpha\alpha'}\Big(\frac{2\pi k}{\lambda}\Big)\rho_{\alpha' k} \cos[\frac{2\pi k}{\lambda} z]]\} \tag{7}$$

where

$$F^{\alpha\alpha'}(q) = \int dz_{12} \cos(q z_{12}) \int dx_{12} dy_{12} f_M^{\alpha\alpha'}(\mathbf{r}_1, \mathbf{r}_2). \tag{8}$$

Note that $F^{\alpha\alpha'}(q = 0)$ is (minus) the excluded volume of a pair of rods with orientations α and α', and that $F^{\alpha\alpha'}(q)$ can be calculated analytically for this particular model. The expansion in Fourier series allows to rewrite the free energy explicitly in terms of the Fourier modes $\rho_{\alpha k}$ and the periodicity λ. In this way one can get the value of λ at fixed density just by minimizing the free energy with respect to this parameter. Isotropic and nematic phase will have $\lambda \to \infty$, whereas $\lambda \simeq H$ in the smectic phase where it denotes the layer spacing. In a numerical implementation of this scheme the summation over the modes is to be truncated beyond a cut-off $k > k_{max}$. In the calculations we performed we set $k_{max} = 10$, which we checked to be sufficient.

With this parameterization of the o.p.d., the following phases can be distinguished:

- In the *isotropic* phase $\rho_{\alpha k} = 0$ for $k \neq 0$ (no z-dependence), and $\rho_{\alpha 0} = 2n/3$ (no orientation dependence) such that $\rho_x(z) = \rho_y(z) = \rho_z(z) = n/3$.

- In the *nematic* phase with director $\hat{z}$ (corresponding to $\alpha = z$) we have $\rho_{\alpha k} = 0$ for $k \neq 0$ (no z-dependence), and $\rho_x(z) = \rho_y(z) = n(1-s)/3$ and $\rho_z(z) = n(1+2s)/3$, with the nematic order parameter $s \in (0, 1]$ that follows numerically from Eq.(7).

- In the *smectic A* phase with director and layer normal $\hat{z}$ we have $\rho_{\alpha k} \neq 0$ for all k, such that $\rho_x(z) = \rho_y(z)$ while the normalization condition

$$\sum_{\alpha} \int_{-\lambda/2}^{\lambda/2} dz \rho_\alpha(z) = n\lambda \tag{9}$$

  is to be satisfied. The scheme to find smectic o.p.d.'s is thus

  1. Guess a value for λ;
  2. Use this value of λ to find the corresponding values of $\rho_{\alpha k}$ by numerically solving the system of Eqs.(6) and (7);
  3. Find the value of λ at which the free energy (3) reaches its minimum; the corresponding $\rho_{\alpha k}$ are the Fourier modes of the o.p.d. of the system at equilibrium.

For a given n we attempt to find isotropic, nematic, and smectic distributions. At low enough n only isotropic distributions can be found, at higher densities also nematic and smectic ones. In Fig. S4 we report some examples of o.p.d. characterized by smectic order. The equilibrium phase diagram follows from e.g. a common tangent construction of the equilibrium free energy density F/V as a function of n, which reveals for the parameter choice $H/D = 4.3$ of present interest an isotropic-smectic A coexistence regime for $0.536 < \eta < 0.566$ where $\eta = nHD^2$ is the packing fraction of the rods. The isotropic-nematic phase coexistence is, for this aspect ratio, metastable. In order to facilitate the visualization of the ISm and IN coexistence the vertical axes of Fig. 3c and 3d in the Letter represent $\eta(F/N - \mu_{ISm})$, where μ_{ISm} is the chemical potential of the isotropic and smectic phase at coexistence (here $\mu_{ISm} = 2.919 k_B T$).

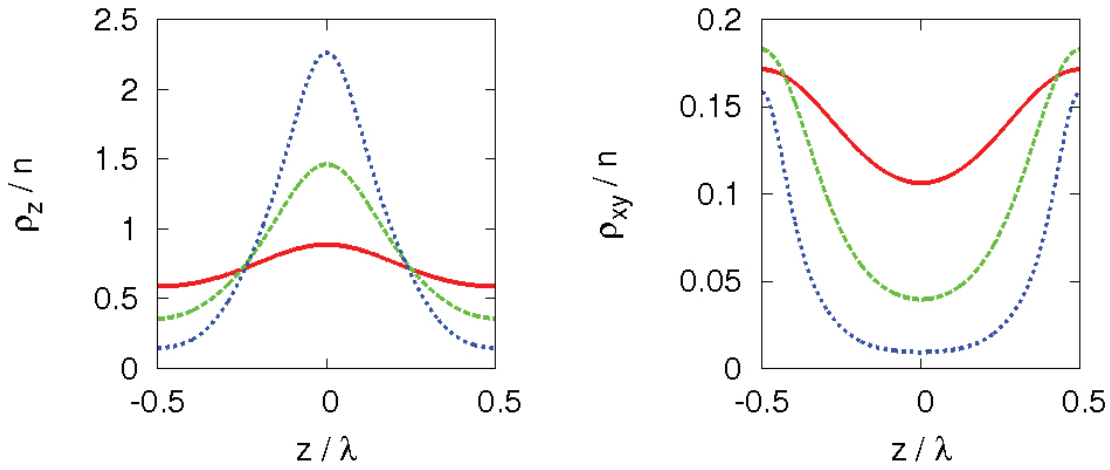

FIG. S4: Scaled smectic one-particle distribution of hard parallelepipeds with aspect ratio $H/D = 4.3$ for orientations parallel (left) and perpendicular (right) to the nematic director, as follows from a second-virial approximation, at packing fraction $\eta = 0.56$ (red solid line), $\eta = 0.60$ (green dashed line) and $\eta = 0.70$ (blue dotted line). The z coordinate is expressed in units of the smectic period ($\lambda/H = 2.17, 1.77, 1.53$, respectively).

C. Bifurcation analysis

The stability of a phase requires that the system is in a state of *minimum* free energy. For a phase with a distribution $\rho_\alpha(\mathbf{r})$ the minimum free-energy condition implies that an arbitrary density fluctuation $h_\alpha(\mathbf{r})$ *increases* $F[\rho]$, in other words that

$$\int d\mathbf{r}d\mathbf{r}' \left.\frac{\delta^2\beta F}{\delta\rho_\alpha(\mathbf{r})\delta\rho_{\alpha'}(\mathbf{r}')}\right|_{\rho_\alpha(\mathbf{r})} h_\alpha(\mathbf{r})h_{\alpha'}(\mathbf{r}') > 0. \tag{10}$$

A spinodal instability occurs at a state (n, T) with an o.p.d. $\rho_\alpha(\mathbf{r})$ such that an infinitessimally small mode $h_\alpha(\mathbf{r})$ exists for which the right hand side of Eq.(10) *equals* zero. Viewing the second functional derivative in Eq.(10) as a matrix operator, we can identify a spinodal instability by a vanishing eigenvalue of the operator, the unstable ("bifurcating") mode being the corresponding eigen-vector or -function [9]. For the present functional (3) a spinodal instability is thus to be analyzed in terms of the eigenvalue problem

$$\frac{\delta^2\beta F}{\delta\rho_\alpha(\mathbf{r})\delta\rho_{\alpha'}(\mathbf{r}')} = \frac{\delta_{\alpha\alpha'}\delta(\mathbf{r}-\mathbf{r}')}{\rho^\alpha(\mathbf{r})} - f_M^{\alpha\alpha'}(\mathbf{r},\mathbf{r}') = 0. \tag{11}$$

Note that at extremely low densities the first (diagonal) term dominates, giving only positive eigenvalues and hence *no* solution such that the state is stable. At higher ρ's instabilities

exist as solutions to Eq.(11). Since in this work we limit to study the stability of the isotropic and nematic phases, which are both homogeneous with $\rho_\alpha(z) = \rho_\alpha$ independent of z, the above matrix equation is more easily solved in Fourier space, where it can be written in terms of an eigenvalue problem as

$$h_\alpha(q) = \rho_\alpha \sum_{\alpha'} F^{\alpha\alpha'}(q) h_{\alpha'}(q), \tag{12}$$

where the kernel $F^{\alpha\alpha'}(q)$ was defined in Eq.(8). The lowest density n (with corresponding isotropic or nematic distribution ρ_α) at which the eigenvalue problem (12) has non trivial solution determines the spinodal point. The IN spinodal is obtained as a $q = 0$ mode for a reference state $\rho_\alpha = n/3$ at $nHD^2 = 0.592$, where the bifurcating eigenvector of the 3×3 problem is $(-1, -1, 2)$, which expresses a nematic order along the third axis. The ISm ($\eta = 0.604$) and the NSm ($\eta = 0.555$) bifurcations give $q \neq 0$ modes, where the periodicity of the smectic phase along the z axis equals $\lambda/H = 2\pi/(qH) = 0.35$ and 2.31 respectively.

---

[1] P.R. ten Wolde and D. Frenkel, J. Chem. Phys. **109**, 901 (1998).

[2] P.R. ten Wolde, M.J. Ruiz-Montero, and D. Frenkel, J. Chem. Phys. **104**, 9932 (1996).

[3] A. Cuetos and M. Dijkstra, Phys. Rev. Lett. **98**, 095701 (2007).

[4] T. Schilling and D. Frenkel, Phys. Rev. Lett. **92**, 085505 (2004).

[5] R. Zwanzig, J. Chem. Phys. **39**, 1714 (1963); K. Shundyak and R. van Roij, Phys. Rev. E **69**, 041703 (2004).

[6] Y. Martinez-Raton and J.A. Cuesta, J. Chem. Phys. **118**, 10164 (2003).

[7] R. van Roij *et al.*, Europhys. Lett. **49**, 350 (2000); M. Dijkstra *et al.*, Phys. Rev. E **63**, 051703 (2001); R. van Roij *et al.*, J. of Chem. Phys. **113**, 7689 (2000).

[8] R. Evans, Adv. Phys. **28**, 143 (1979).

[9] R.F. Kayser and H.J. Raveché, Phys. Rev. A. **17**, 2067 (1978); B.M. Mulder, Phys. Rev. A. **39**, 360 (1987).